ACS Photonics

Letter

pubs.acs.org/journal/apchd5

Nonlinear Polariton Localization in Strongly Coupled Driven-Dissipative Microcavities

Said Rahimzadeh Kalaleh Rodriguez,*[,†,¶] Alberto Amo,[†] Iacopo Carusotto,[‡] Isabelle Sagnes,[†] Luc Le Gratiet,[†] Elisabeth Galopin,[†] Aristide Lemaitre,[†] and Jacqueline Bloch[†]

[†]Centre de Nanosciences et de Nanotechnologies, CNRS, Université Paris-Sud, Université Paris-Saclay, C2N—Marcoussis, 91460 Marcoussis, France

[‡]INO—CNR BEC Center and Dipartimento di Fisica, Università di Trento, I-38123 Povo, Italy

ABSTRACT: The interplay of hopping and interactions in coupled photonic resonators gives rise to a number of nonlinear optical phenomena including multistability, self-trapping, and nonlinear Josephson oscillations. Here we use two coupled semiconductor microcavities to investigate the nonlinear localization of polaritons in a novel regime where a single cavity is coherently driven at a frequency just above the lowest bonding state of the dimer. For driving powers above the bistability threshold we observe that polaritons progressively localize in the driven cavity. Our experimental observations are reproduced by numerical calculations using a one-dimensional driven-dissipative Gross—Pitaevskii equation. The phenomenology here observed shows the potential of nonlinear coupled photonic resonators to engineer novel optical functionalities.

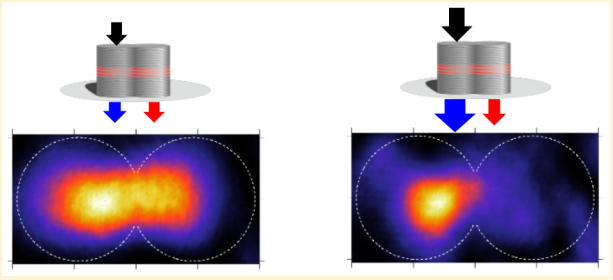

KEYWORDS: *exciton—polaritons, nonlinear, coupled cavities, optical bistability, localization*

The strong light—matter coupling (SLMC) regime, wherein subsystems exchange optical and material excitations faster than they dissipate, is attracting increasing interest at the crossroads between physics, chemistry, materials science, and biology.[1−5] SLMC enables the combination of photonic and material excitations to produce novel physical properties and functionalities. From an optics standpoint, SLMC is opening new perspectives for controlling the flow of light,[6−8] for inducing lasing,[9,10] and for enhancing nonlinear effects.[11−13] Particularly promising is the study of nonlinear optical properties induced by the matter part of polaritons, the fundamental quasiparticles of systems in the SLMC regime. Semiconductor microcavities are a convenient platform to explore nonlinear effects in engineered landscapes. For instance, single micropillars have been used to produce optical intensity squeezing,[14] parametric oscillation,[15] and polarization multistability.[16] In dimers of coupled microcavities, self-trapping and nonlinear Josephson oscillations[17] and spatial multistability[18] have been observed. Moreover, single-photon emission[19] and a rich phenomenology associated with parity-time symmetry[20] in coupled nonlinear resonators have been predicted. In this Letter, we reveal a novel nonlinear effect in two-coupled driven-dissipative microcavity micropillars: we demonstrate how the equidistributed density profile associated with the lowest energy steady state of this dimer is reshaped due to effective photon—photon interactions, with polaritons being progressively localized in one of the two coupled cavities. This reshaping occurs above the regime of mean-field bistability, wherein two stable steady states can be observed for a single driving condition.

SAMPLE AND SETUP

The inset of Figure 1(a) shows an inclined-view scanning electron micrograph of the sample under study. This semiconductor microstructure is shaped in the form of two slightly overlapping cylinders representing two coupled microcavities. This photonic dimer was engineered using e-beam lithography and dry etching starting from a planar microcavity grown by molecular beam epitaxy. The microcavity structure includes a GaAs λ planar spacer sandwiched between two distributed Bragg reflectors (DBRs) made out of alternating $\lambda/4$ layers of $Ga_{0.9}Al_{0.1}As$ and $Ga_{0.05}Al_{0.95}As$. The top and bottom DBRs have 26 and 30 pairs, respectively. At the center of the cavity there is a single 8 nm $In_{0.04}Ga_{0.96}As$ quantum well supporting excitons with an energy of 1480.7 meV. Strong exciton—photon coupling leads to a Rabi splitting of 3.4 meV, a hundred times larger than the lower polariton line width (37 μeV). Based on the bare exciton energy and on the Rabi splitting, we estimate a photon fraction of $|C|^2 = 0.84 \pm 0.03$ for polaritons at the energy of the antibonding resonance.[18]

For all experiments the sample was held in a closed-cycle cryostat at 4 K. A single-mode continuous wave laser focused

Special Issue: Strong Coupling of Molecules to Cavities

Received: July 4, 2017
Published: October 23, 2017

DOI: 10.1021/acsphotonics.7b00721
ACS Photonics 2018, 5, 95−99

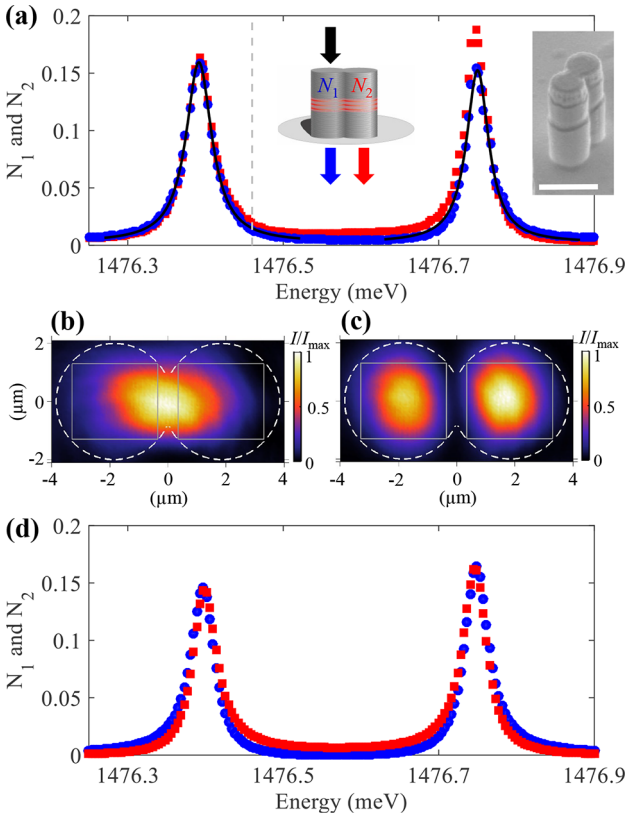

Figure 1. (a) Measured mean number of polaritons in the driven (blue dots) and undriven (red dots) cavity as a function of the energy of the driving laser, at a fixed power in the linear regime. The black lines are Lorentzian fits to deduce the mode energies and line widths. The right inset is a scanning electron micrograph of the semiconductor structure under study. The dashed gray line indicates the driving energy considered throughout Figures 2, 3, and 4. (b and c) Normalized spatially resolved transmission at the low- and high-energy peak in (a), respectively. The gray squares show the integration areas. (d) Calculated steady-state polariton populations in the double-well potential shown in Figure 4(d). The population in the left well (the driven site) is represented by the blue dots, and the population in the right well is represented by the red squares.

on a spot of 1 μm in diameter drives one of the cavities of the dimer. The excitation laser beam is linearly polarized parallel to the dimer axis [horizontal line at 0 μm in Figures 1(b,c)]. The transmitted intensity of the entire structure is recorded with a CCD camera. The excitation and collection objectives have a numerical aperture of 0.5 and 0.4, respectively.

RESULTS

Figure 1(a) shows the cavity-resolved transmission spectrum under weak driving, i.e., in the linear regime, when integrating the emission from the driven (blue dots) and undriven (red squares) cavities. The low- and high-energy peaks in Figure 1(a) correspond to bonding and antibonding polariton resonances, arising from the symmetric and antisymmetric superposition of the uncoupled polariton ground states.[21] Figure 1(b) and (c) show the spatially resolved transmission at the peak energy of the bonding and antibonding resonances, respectively. The vanishing density at the center of the dimer in Figure 1(c) reflects the odd parity of the antibonding mode wave function. In contrast, the significant density at the center of the dimer in Figure 1(b) reflects the even parity of the bonding mode wave function. The left and right squares in Figures 1(b,c) indicate the integration areas within which the transmitted intensity is ascribed to the driven and undriven cavity, respectively. The same integration domains were used for all values of the driving energy and intensity considered throughout this Letter.

Next, we investigate the nonlinear regime by driving the left cavity with increasing power. Figure 2(a) shows the

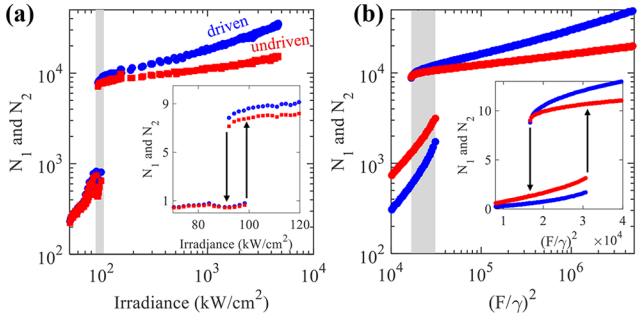

Figure 2. (a) Measured cavity-resolved mean number of polaritons as a function of the laser irradiance for a fixed driving energy of 1476.46 meV, indicated by the dashed line in Figure 1(a). (b) Calculated steady-state polariton populations in the double-well potential shown in Figure 4(d), at the same driving energy used for the experiments in (a). In both (a) and (b) the shaded area indicates the bistability range, and the inset shows a zoom-in of it.

experimentally measured cavity-resolved polariton occupations as a function of the irradiance. For these measurements we scanned the driving power up and down at a fixed energy indicated by the gray dashed line in Figure 1(a). To estimate the occupation, we measured the absolute photon intensity emitted by each cavity following the procedure described in ref 18. Two main features are observed in the experiment. First, we report a range of irradiance (shaded area in Figure 2(a)) for which we observe two states with different photon numbers at the same irradiance, i.e., bistability.[22] The inset of Figure 2(a) shows a zoom-in on the bistability and the associated optical hysteresis. The arrows indicate the direction of the density jumps when scanning the power across the bistability. Second, for increasing intensities above the bistability range, the population in the driven cavity (blue dots in Figure 2(a)) grows at a faster rate than the population in the undriven cavity (red squares). In other words, the polariton population localizes in the driven cavity.

We now focus on the intensity-induced polariton localization. Figure 3 shows the spatially resolved transmission at three different powers above the bistability range when driving the left cavity. Figure 3(a) shows the transmission at 0.19×10^3 kW/cm^2, just above the bistability range. The density profile observed in Figure 3(a) resembles the one observed for the bonding mode (linear regime) in Figure 1(a). This resemblance is due to the fact that, just above the bistability range, repulsive polariton−polariton interactions blue-shift the bonding mode and bring it in resonance with the driving laser. Interestingly, in Figure 3(a), a small imbalance in favor of the driven (left) cavity can already be observed. For greater powers, Figure 3(b,c) show increasing localization of the polariton density in the driven cavity. The nonlinear localization in the driven cavity is further demonstrated in Figure 4(a) for a wider range of powers, where each profile shows the emitted intensity

DOI: 10.1021/acsphotonics.7b00721
ACS Photonics 2018, 5, 95−99

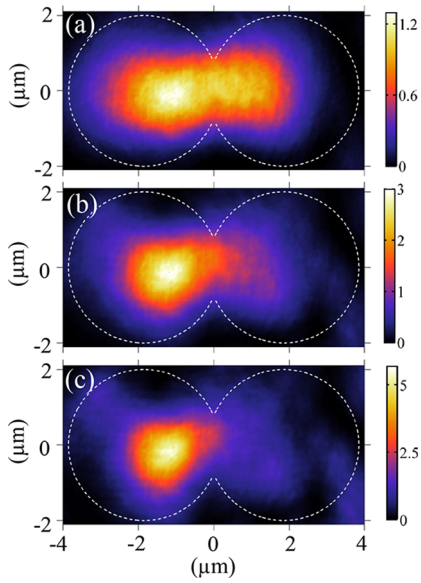

Figure 3. Spatially resolved transmitted intensity at a fixed driving energy of 1476.46 meV (same as in Figures 2 and 4) and for an irradiance of (a) 0.19×10^3 kW/cm^2, (b) 1.5×10^3 kW/cm^2, and (c) 4.6×10^3 kW/cm^2.

integrated over an horizontal band of 2 μm width (1 μm above and 1 μm below the dimer axis).

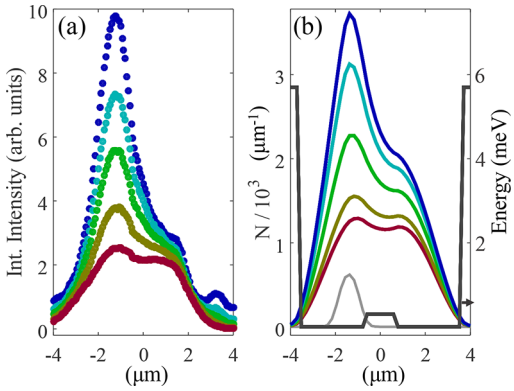

Figure 4. (a) Measured intensity along the dimer axis for five distinct driving powers, all at a fixed driving energy of 1476.46 meV (same as in Figures 2 and 3). The transmitted intensity was integrated along the direction perpendicular to the dimer axis, over a total width of 2 μm. The irradiance increases for each curve from bottom to top: 92×10^3 kW/cm^2, 190×10^3 kW/cm^2, 890×10^3 kW/cm^2, 2660×10^3 kW/cm^2, and 4640×10^3 kW/cm^2. (b) Calculated steady-state polariton populations in the double-well potential shown as a black line (see right axis for units). From bottom to top, the values of $(F/\gamma)^2$ used in the calculations are 0.115×10^5, 0.237×10^5, 1.11×10^5, 3.31×10^5, and 5.78×10^5. The gray curve in (b) indicates the Gaussian profile (in arb. units) of the driving beam used for all calculations in the text. In both experiments and theory, the plotted curves correspond to powers $(1.0, 2.1, 9.7, 28, 50)P_0$, where P_0 is the power corresponding to the lowest curve.

Both the low power transmission and the high power regime associated with bistability and nonlinear localization can be modeled using an effective 1D driven-dissipative Gross–Pitaevskii equation for the polariton wave function $\psi(x,t)$:

$$i\hbar\frac{\partial\psi(x,t)}{\partial t} = \left[E_0 - \frac{\hbar^2}{2m}\frac{\partial^2}{\partial x^2} + V(x) + U|\psi|^2\right] \times \psi(x,t) - i\frac{\gamma}{2}\psi(x,t) + F(x)e^{-i\omega t} \quad (1)$$

The driven-dissipative Gross–Pitaevskii equation is a mean-field model neglecting quantum fluctuations. It has been widely used to describe nonlinear dynamics of polaritons, including superfluidity and the nucleation of vortices and solitons.[7] Here, we set the model parameters as explained next. The line width was set to $\gamma = 37$ μeV based on Lorentzian fits to the measured line shapes in the linear regime [see black lines in Figure 1(a)]. The potential energy function $V(x)$ and the driving beam $F(x)$ profile are indicated by the dark and light gray lines in Figure 4(b), respectively. $V(x)$ defines a double-well potential, each well representing a pillar microcavity. To match the calculated spectrum in the low power limit to the experimental one, we set the energy offset to $E_0 = 1476.163$ meV, and we fine-tuned the height of the barrier between the wells. The barrier height determines the tunneling rate J between the wells, which in turn sets the bonding–antibonding energy splitting $2J$. Comparison of Figure 1(d) and (a) shows excellent agreement between the measured and calculated spectra, validating our choice of linear parameters.

The interaction energy was set to $U = 0.07$ μeV·μm to match the calculated and measured polariton occupations in the nonlinear regime depicted in Figure 2(b) and Figure 4(b). The simulations reproduce both the measured transmission displayed in Figure 2(a) and the spatial profiles of Figure 4(a). The agreement between experiment and simulations, in reproducing the progressive localization in the driven cavity at high irradiance, highlights the validity of the description based on a 1D effective model. Small discrepancies between experiments and theory are likely related to how the selected integration areas [gray squares in Figure 1(b,c)] influence the counts attributed to one cavity or another. In other words, our estimated location of the center of the dimer, and hence the positions of the integration areas, could be slightly off. Such an error could counteract a small population imbalance between cavities, such that no population imbalance is detected for low irradiances as in Figure 2(a).

The value of the effective 1D interaction energy used to fit our experiments can be approximately converted to a 2D interaction energy as follows: $U_{2D} = U\sqrt{A}$, where A is the microcavity cross-sectional area. For the microcavities under study we have $A = 11.3$ μm^2, such that $U_{2D} = 0.8$ μeV·μm^2; this is the same value reported for the two-dimensional polariton–polariton interaction constant in our earlier work.[18] As explained in ref 18, an exciton–exciton interaction energy of $g_{exc} = 30$ μeV·μm^2 is obtained from $U_{2D} = 0.8$ μeV·μm^2 by taking into account the exciton fraction of the polariton.

The localization of the polariton density in the driven cavity for increasing pumping intensities can be qualitatively understood from the linear transmission characteristics. The spectra in Figure 1(a,d) show that, in the linear regime, the driven cavity has higher density than the undriven one throughout the low-energy side of the bonding mode (blue dots stay above the red squares below the bonding mode resonance). The difference in transmission gets larger for lower energies.

For a driving energy just above the bonding mode resonance, on the upper branch of the bistability loop, repulsive polariton–polariton interactions blue-shift the bonding mode across the

DOI: 10.1021/acsphotonics.7b00721
ACS Photonics 2018, 5, 95–99

laser energy so that its low-energy side remains on resonance with the laser. This results in a higher transmission for the driven cavity, with an increasing differential transmission of the driven and undriven cavities as the intensity grows.

The situation is reversed on the lower energy side of the *antibonding* mode. In that case, the *undriven* cavity presents a higher transmission than the driven one. When pumping close to the antibonding resonance, the nonlinear blue-shifts result this time in a darkening of the driven cavity as reported in ref 18. Therefore, by tuning the driving energy, the interplay between interactions (blue-shift) and destructive/constructive interference effects can be used to induce the nonlinear antilocalization (around the antibonding mode; ref 18) or localization (around the bonding mode; this work) of polaritons in a dimer.

Finally, we would like to point out that the nonlinear localization of polaritons here reported is unaffected by quantum (or other) fluctuations because they occur for driving powers above the bistability. In this regime, quantum fluctuations around a mean-field steady state are in fact negligibly small.[7] Fluctuation-induced switching events between different steady states are only relevant in the power range where mean-field and quantum theories disagree in respectively predicting bistability or a unique steady state. In that range, fluctuations can trigger switching between mean-field steady states and reduce the hysteresis area,[23] so that for an infinitely slow sweep of the driving power the hysteresis area associated with the bistability vanishes. These effects have recently been connected to a dissipative phase transition.[23,24] While a coupled cavity system similar to the one employed in this work could serve to explore the physics associated with fluctuations and dissipative phase transitions in nonlinear resonators, we would need to adjust the driving frequency and/or the polariton−polariton interaction strength significantly. In our present configuration, a mean-field theory ignoring quantum fluctuations suffices to reproduce our experimental observations.

CONCLUSION

To summarize, we have studied the influence of nonlinear interactions on the bonding mode of two strongly coupled driven-dissipative microcavities. At high driving powers, above the regime of mean-field bistability, we have observed a pronounced localization of polaritons in the driven site. We expect similar effects to arise in complex multicavity systems for which numerous exciting predictions have been made,[25−29] yet experiments at optical frequencies remain scarce. Nonlinear localization of polaritons may also be observed in dimer lattices where interactions can lead to nontrivial topological phases[30] or in trimer lattices supporting flat energy bands.[31,32] In addition, recent experiments have shown the possibility to achieve lasing from edge states in dimer lattices.[33] The nonlinear phenomena reported here are also promising for the study of PT-symmetry-related effects when pumping the system nonresonantly. Our results are relevant to these emerging fields of fundamental research in photonics, as well as to technological applications involving coupled nonlinear cavities which may function as optical memories or switches.

AUTHOR INFORMATION

Corresponding Author

*E-mail: s.rodriguez@uu.nl.

ORCID

Said Rahimzadeh Kalaleh Rodriguez: 0000-0003-3761-3137

Present Address

[¶]Nanophotonics, Debye Institute, Utrecht University, P.O. Box 80.000, 3508 TA Utrecht, The Netherlands.

Notes

The authors declare no competing financial interest.

ACKNOWLEDGMENTS

This work was supported by the Marie Curie individual fellowship PINQUAR (Project No. 657042), the French National Research Agency (ANR) program Labex NanoSaclay via the projects ICQOQS (ANR-10-LABX-0035) and Quantum Fluids of Light (ANR-16-CE30-0021), the French RENATECH network, the ERC grant Honeypol, and the EU-FET Proactiv grant AQUS (Project No. 640800).

REFERENCES

(1) Orgiu, E.; George, J.; Hutchison, J. A.; Devaux, E.; Dayen, J. F.; Doudin, B.; Stellacci, F.; Genet, C.; Schachenmayer, J.; Genes, C.; Pupillo, G.; Samori, T. P.; Ebbesen. Conductivity in organic semiconductors hybridized with the vacuum field. *Nat. Mater.* **2015**, *14*, 1123−1129.

(2) Galego, J.; Garcia-Vidal, F. J.; Feist, J. Cavity-Induced Modifications of Molecular Structure in the Strong-Coupling Regime. *Phys. Rev. X* **2015**, *5*, 041022.

(3) Zeng, P.; Cadusch, J.; Chakraborty, D.; Smith, T. A.; Roberts, A.; Sader, J. E.; Davis, T. J.; Gómez, D. E. Photoinduced Electron Transfer in the Strong Coupling Regime: Waveguide-Plasmon Polaritons. *Nano Lett.* **2016**, *16*, 2651−2656.

(4) Coles, D. M.; Yang, Y.; Wang, Y.; Grant, R. T.; Taylor, R. A.; Saikin, S. K.; Aspuru-Guzik, A.; Lidzey, D. G.; Tang, J. K.-H.; Smith, J. M. Strong coupling between chlorosomes of photosynthetic bacteria and a confined optical cavity mode. *Nat. Commun.* **2014**, *5*, 556110.1038/ncomms6561.

(5) Tsargorodska, A.; Cartron, M. L.; Vasilev, C.; Kodali, G.; Mass, O. A.; Baumberg, J. J.; Dutton, P. L.; Hunter, C. N.; Törmä, P.; Leggett, G. J. Strong Coupling of Localized Surface Plasmons to Excitons in Light-Harvesting Complexes. *Nano Lett.* **2016**, *16*, 6850−6856.

(6) Amo, A.; Lefrère, J.; Pigeon, S.; Adrados, C.; Ciuti, C.; Carusotto, I.; Houdré, R.; Giacobino, E.; Bramati, A. Superfluidity of polaritons in semiconductor microcavities. *Nat. Phys.* **2009**, *5*, 805.

(7) Carusotto, I.; Ciuti, C. Quantum fluids of light. *Rev. Mod. Phys.* **2013**, *85*, 299−366.

(8) Lerario, G.; Fieramosca, A.; Barachati, F.; Ballarini, D.; Daskalakis, K. S.; Dominici, L.; De Giorgi, M.; Maier, S. A.; Gigli, G.; Kéna-Cohen, S.; Sanvitto, D. Room-temperature superfluidity in a polariton condensate. *Nat. Phys.* **2017**, *13*, 837.

(9) Dietrich, C. P.; Steude, A.; Tropf, L.; Schubert, M.; Kronenberg, N. M.; Ostermann, K.; Höfling, S.; Gather, M. C. An exciton-polariton laser based on biologically produced fluorescent protein *Sci. Adv.* **2016**, *2*, e160066610.1126/sciadv.1600666.

(10) Ramezani, M.; Halpin, A.; Fernández-Domínguez, A. I.; Feist, J.; Rodriguez, S. R.-K.; Garcia-Vidal, F. J.; Rivas, J. G. Plasmon-exciton-polariton lasing. *Optica* **2017**, *4*, 31−37.

(11) Chervy, T.; Xu, J.; Duan, Y.; Wang, C.; Mager, L.; Frerejean, M.; Münninghoff, J. A. W.; Tinnemans, P.; Hutchison, J. A.; Genet, C.; Rowan, A. E.; Rasing, T.; Ebbesen, T. W. High-Efficiency Second-Harmonic Generation from Hybrid Light-Matter States. *Nano Lett.* **2016**, *16*, 7352−7356.

(12) del Pino, J.; Garcia-Vidal, F. J.; Feist, J. Exploiting Vibrational Strong Coupling to Make an Optical Parametric Oscillator Out of a Raman Laser. *Phys. Rev. Lett.* **2016**, *117*, 277401.

(13) Barachati, F.; Simon, J.; Getmanenko, Y. A.; Marder, S. R.; Kéna-Cohen, S. Tunable third-harmonic generation from polaritons in the ultrastrong coupling regime. arXiv:1703.08536, 2017.

DOI: 10.1021/acsphotonics.7b00721
ACS Photonics 2018, 5, 95−99

(14) Boulier, T.; Bamba, M.; Amo, A.; Adrados, C.; Lemaitre, A.; Galopin, E.; Sagnes, I.; Bloch, J.; Ciuti, C.; Giacobino, E.; Bramati, A. Polariton-generated intensity squeezing in semiconductor micropillars. *Nat. Commun.* **2014**, *5*, No. 3260.
(15) Ferrier, L.; Pigeon, S.; Wertz, E.; Bamba, M.; Senellart, P.; Sagnes, I.; Lemaître, A.; Ciuti, C.; Bloch, J. Polariton parametric oscillation in a single micropillar cavity. *Appl. Phys. Lett.* **2010**, *97*, 031105.
(16) Paraïso, T.; Wouters, M.; Léger, Y.; Morier-Genoud, F.; Deveaud-Plédran, B. Multistability of a coherent spin ensemble in a semiconductor microcavity. *Nat. Mater.* **2010**, *9*, 655−660.
(17) Abbarchi, M.; Amo, A.; Sala, V.; Solnyshkov, D.; Flayac, H.; Ferrier, L.; Sagnes, I.; Galopin, E.; Lemaître, A.; Malpuech, G.; Bloch, J. Macroscopic quantum self-trapping and Josephson oscillations of exciton polaritons. *Nat. Phys.* **2013**, *9*, 275−279.
(18) Rodriguez, S.; Amo, A.; Sagnes, I.; Le Gratiet, L.; Galopin, E.; Lemaitre, A.; Bloch, J. Interaction-induced hopping phase in driven-dissipative coupled photonic microcavities. *Nat. Commun.* **2016**, *7*, 11887.
(19) Liew, T. C. H.; Savona, V. Single Photons from Coupled Quantum Modes. *Phys. Rev. Lett.* **2010**, *104*, 183601.
(20) Lien, J.-Y.; Chen, Y.-N.; Ishida, N.; Chen, H.-B.; Hwang, C.-C.; Nori, F. Multistability and condensation of exciton-polaritons below threshold. *Phys. Rev. B: Condens. Matter Mater. Phys.* **2015**, *91*, 024511.
(21) Galbiati, M.; Ferrier, L.; Solnyshkov, D. D.; Tanese, D.; Wertz, E.; Amo, A.; Abbarchi, M.; Senellart, P.; Sagnes, I.; Lemaître, A.; Galopin, E.; Malpuech, G.; Bloch, J. Polariton Condensation in Photonic Molecules. *Phys. Rev. Lett.* **2012**, *108*, 126403.
(22) Baas, A.; Karr, J. P.; Eleuch, H.; Giacobino, E. Optical bistability in semiconductor microcavities. *Phys. Rev. A: At., Mol., Opt. Phys.* **2004**, *69*, 023809.
(23) Rodriguez, S. R. K.; Casteels, W.; Storme, F.; Carlon Zambon, N.; Sagnes, I.; Le Gratiet, L.; Galopin, E.; Lemaître, A.; Amo, A.; Ciuti, C.; Bloch, J. Probing a Dissipative Phase Transition via Dynamical Optical Hysteresis. *Phys. Rev. Lett.* **2017**, *118*, 247402.
(24) Demirchyan, S. S.; Khudaiberganov, T. A.; Chestnov, I. Y.; Alodzhants, A. P. Quantum fluctuations in a system of exciton polaritons in a semiconductor microcavity. *J. Opt. Technol.* **2017**, *84*, 75−81.
(25) Le Boité, A.; Orso, G.; Ciuti, C. Steady-State Phases and Tunneling-Induced Instabilities in the Driven Dissipative Bose-Hubbard Model. *Phys. Rev. Lett.* **2013**, *110*, 233601.
(26) Hartmann, M. J. Quantum simulation with interacting photons. *J. Opt.* **2016**, *18*, 104005.
(27) Noh, C.; Angelakis, D. G. Quantum simulations and many-body physics with light. *Rep. Prog. Phys.* **2017**, *80*, 016401.
(28) Wilson, R. M.; Mahmud, K. W.; Hu, A.; Gorshkov, A. V.; Hafezi, M.; Foss-Feig, M. Collective phases of strongly interacting cavity photons. *Phys. Rev. A: At., Mol., Opt. Phys.* **2016**, *94*, 033801.
(29) Foss-Feig, M.; Niroula, P.; Young, J. T.; Hafezi, M.; Gorshkov, A. V.; Wilson, R. M.; Maghrebi, M. F. Emergent equilibrium in many-body optical bistability. *Phys. Rev. A: At., Mol., Opt. Phys.* **2017**, *95*, 043826.
(30) Hadad, Y.; Khanikaev, A. B.; Alù, A. Self-induced topological transitions and edge states supported by nonlinear staggered potentials. *Phys. Rev. B: Condens. Matter Mater. Phys.* **2016**, *93*, 155112.
(31) Baboux, F.; Ge, L.; Jacqmin, T.; Biondi, M.; Galopin, E.; Lemaître, A.; Le Gratiet, L.; Sagnes, I.; Schmidt, S.; Türeci, H. E.; Amo, A.; Bloch, J. Bosonic Condensation and Disorder-Induced Localization in a Flat Band. *Phys. Rev. Lett.* **2016**, *116*, 066402.
(32) Whittaker, C.; Cancellieri, E.; Walker, P.; Gulevich, D.; Schomerus, H.; Vaitiekus, D.; Royall, B.; Whittaker, D.; Clarke, E.; Iorsh, I.; Shelykh, I. A.; Skolnick, M. S.; Krizhanovskii, D. N. Exciton-polaritons in a two-dimensional Lieb lattice with spin-orbit coupling. arXiv:1705.03006, **2017**.
(33) St-Jean, P.; Goblot, V.; Galopin, E.; Lemaître, A.; Ozawa, T.; Gratiet, L. L.; Sagnes, I.; Bloch, J.; Amo, A. Lasing in topological edge states of a one-dimensional lattice. *Nat. Photonics* **2017**, *11*, 651.

DOI: 10.1021/acsphotonics.7b00721
ACS Photonics 2018, 5, 95−99